

Optical Studies of Thirteen Hard X-ray Selected Cataclysmic Binaries from the *Swift*-BAT Survey¹

Jules P. Halpern

Columbia Astrophysics Laboratory, Columbia University, 550 West 120th Street, New York, NY 10027, USA

John R. Thorstensen

Department of Physics and Astronomy, Dartmouth College, Hanover NH, 03755, USA

ABSTRACT

From a set of thirteen cataclysmic binaries that were discovered in the *Swift* Burst Alert Telescope (BAT) survey, we conducted time-resolved optical spectroscopy and/or time-series photometry of eleven, with the goal of measuring their orbital periods and searching for spin periods. Seven of the objects in this study are new optical identifications. Orbital periods are found for seven targets, ranging from 81 minutes to 20.4 hours. PBC J0706.7+0327 is an AM Herculis star (polar) based on its emission-line variations and large amplitude photometric modulation on the same period. Swift J2341.0+7645 may be a polar, although the evidence here is less secure. Coherent pulsations are detected from two objects, Swift J0503.7–2819 (975 s) and Swift J0614.0+1709 (1412 s and 1530 s, spin and beat periods, respectively), indicating that they are probable intermediate polars (DQ Herculis stars). For two other stars, longer spin periods are tentatively suggested. We also present the discovery of a 2.00 hour X-ray modulation from RX J2015.6+3711, possibly a contributor to Swift J2015.9+3715, and likely a polar.

Subject headings: novae, cataclysmic variables — X-rays: binaries — stars: individual (PBC J0325.6–0820, Swift J0503.7–2819, Swift J0525.6+2416, Swift J0614.0+1709, Swift J0623.9–0939, PBC J0706.7+0327, Swift J0717.8–2156, Swift J0749.7–3218, Swift J0820.6–2805, Swift J0939.7–3224, 4PBC J1740.7+0603, RX J2015.6+3711, Swift J2124.6+0500, Swift J2341.0+7645)

1. INTRODUCTION

Cataclysmic variables (CVs) are accreting binaries in which a dwarf star donates mass to a white dwarf (WD) via Roche-lobe overflow. CVs such as dwarf novae are often discovered in

¹Based on observations obtained at the MDM Observatory, operated by Dartmouth College, Columbia University, Ohio State University, Ohio University, and the University of Michigan.

outburst by large-scale optical time-domain surveys. Ultraviolet and X-ray surveys find CVs in all states of luminosity. Hard X-ray energies (> 15 keV) preferentially select systems in which the magnetic field of the WD is strong enough to truncate the accretion disk at a magnetospheric boundary, or prevent it from forming completely. In these systems, an accretion column is channeled onto the magnetic pole(s), where thermal bremsstrahlung X-rays are radiated from a shock just above the surface of the WD.

In polars (AM Herculis stars), the magnetic field is strong enough to channel matter directly from the companion, and the WD rotation is locked to the binary orbit, or nearly so in the few asynchronous polars. Polars are also characterized by their optical circular polarization, and optical/IR humps in their spectra from cyclotron radiation in the strong magnetic field. Intermediate polars (IPs, or DQ Herculis stars) have weaker magnetic fields and a truncated accretion disk. The spin period of the WD in an IP is detected as a coherent oscillation in X-ray or optical emission from a rotating hot spot, at a shorter period than the orbital period of the binary. Sometimes the beat period between the spin and orbit periods is seen, due to reprocessed emission.

We have been studying newly discovered CVs and CV candidates from the hard X-ray surveys of the *International Gamma-Ray Astrophysics Laboratory (INTEGRAL)*/IBIS, and the *Swift* Burst Alert Telescope (BAT), using time-resolved optical spectroscopy to measure their orbital periods, and time-series photometry to search for spin and/or orbital modulation. The Swift-BAT 70 month hard X-ray survey (Baumgartner et al. 2013) lists 55 CVs, of which 41 are magnetic: 31 IPs and 10 polars. IPs outnumber polars in hard X-ray surveys, presumably because of their higher accretion rates, and also because in polars the accretion may be more “blobby,” depositing some fraction of the energy directly onto the surface of the WD, which is radiated at temperatures of tens of eV.

In Thorstensen & Halpern (2013, hereafter Paper I), we presented data and findings on 10 hard X-ray selected CVs, three of which were unidentified X-ray sources prior to our work. The present paper continues this effort with information on another thirteen objects. In particular, we now concentrate on the unclassified *Swift*-BAT sources, of which there are 88, including the 23 indicated simply as “Galactic” based on their coordinates.

The targets were selected based on their accessibility from the northern hemisphere, and properties likely to favor magnetic CVs. Spectral information from the literature was consulted. Unidentified *Swift*-BAT sources, for which we examined pointed observations with the *Swift* X-ray Telescope (XRT) and UV/Optical Telescope (UVOT), were chosen if they had bright, variable counterparts in the XRT and/or a relatively bright and/or blue optical counterpart in the UVOT. These criteria were found to be uniformly successful in identifying CVs. In addition, we identified several non-variable X-ray sources with fainter optical counterparts as active galactic nuclei, which will be reported elsewhere. This paper identifies seven new CV counterparts, as well as characterizing six that were previously identified spectroscopically but lack detailed studies in the literature. We also present in an Appendix an X-ray result on a CV that may have been detected in hard X-rays.

2. EQUIPMENT AND TECHNIQUES

Our instrumentation, and reduction and analysis procedures are essentially identical to those described in Paper I, and are summarized in this section. All of our optical data are from the MDM Observatory, which comprises the 1.3 m McGraw-Hill telescope and the 2.4 m Hiltner telescope, both on the southwest ridge of Kitt Peak, Arizona. With a single exception, the radial velocity studies to search for the orbital periods were done on the 2.4 m, while high-cadence photometry sensitive to spin periods was carried out on the 1.3 m.

2.1. Spectroscopy

All of our radial velocity studies used the modular spectrograph, as described in Paper I. In addition to wavelength calibrations using comparison lamps of Hg, Ne, and Xe taken during twilight, we used the night-sky O I λ 5577 line to track and correct for spectrograph flexure during the night. Most of our velocities are from the the 2.4m telescope, where we rotated the instrument to orient the slit close to the parallactic angle when at large hour angles and zenith distances. Although the 1'' projected slit width does not permit accurate spectrophotometry, flux standards were applied to the spectra, with an expected accuracy of $\sim 20\%$ for the averages spectra suggested by experience. Some spectra of Swift J2124.6+0500, and all the data we used for Swift J0939.7–3224, are from the McGraw-Hill 1.3m telescope, again with the modular spectrograph. At the 1.3m telescope, we left the spectrograph slit oriented north-south for all observations.

We reduced our spectra using Pyraf scripts that for the most part called IRAF² tasks. To extract one-dimensional spectra, we implemented the algorithm published by Horne (1986). We measured emission-line radial velocities using convolution algorithms described by Schneider & Young (1980) and Shafter (1983). To measure synthetic magnitudes from our spectra we used the Bessell (1990) tabulation of the V passband and the IRAF `sbands` task.

To search for periods in the spectroscopic time series, we used a “residual-gram” algorithm (Thorstensen et al. 1996). Observing constraints sometimes led to ambiguities in the daily cycle count. To resolve them, we used the Monte Carlo method of Thorstensen & Freed (1985), which employs the “discriminatory power” statistic, which is the fraction of Monte Carlo trials that result in the correct period being chosen, rather than an alias, by virtue of having the smallest residuals.

For four newly identified objects we have only single spectra that were obtained on two observing runs on the 2.4m. These used the Boller and Chivens CCD spectrograph (CCDS) and the Ohio State Multi-Object Spectrograph (OSMOS). Descriptions of these instruments can be found

²IRAF is distributed by the National Optical Astronomy Observatory, which is operated by the Association of Universities for Research in Astronomy (AURA) under cooperative agreement with the National Science Foundation.

on the MDM Observatory web page³.

2.2. Time-Series Photometry

Most of the time-series photometry used “Templeton”, a thinned, back-illuminated SITe CCD with 1024×1024 24μ pixels, each subtending $0.''508$ at the 1.3 m. To minimize read time, the readout was usually windowed and binned 2×2 . Exposures ranged from 10–30 s, with 3 s dead-time between exposures. For one star, we used the thermoelectrically cooled Andor Ikon DU-937N CCD camera as described in Paper I. It has a dead-time of only 11.92 ms when binned 4×4 to give a pixel size of $1.''1$. Filters used were V for bright stars or, more commonly, broadband Schott BG38 or GG420 to maximize throughput for fainter stars. BG38 passes a broad band from roughly 3250 to 6500 Å, with a significant red leak. GG420 is a long-pass filter transmitting $\lambda > 4200$ Å that is useful for suppressing scattered moonlight.

Differential photometry with respect to a single comparison star that was typically 2–4 mag brighter than the variable was performed using the IRAF task `phot`. Approximate magnitudes were derived for the BG38 filter by averaging the B and R magnitudes of the comparison star in the USNO B1.0 catalog (Monet et al. 2003), or adopting the R magnitude of the comparison star in the GG420 filter. Sequences on individual stars ranged from 1.9–9.6 hours. Period searches used a standard power-spectrum analysis on these evenly sampled light curves.

3. RESULTS ON INDIVIDUAL OBJECTS

The objects observed are listed in Table 1, which provides accurate celestial coordinates, approximate magnitudes, and spin periods where discovered. Figure 1 gives finding charts of the objects for which we have our own direct images. Table 2 lists the radial velocity data, and Table 3 gives parameters of the best-fit sinusoids. Figures 2 and 3 show mean spectra, radial velocity periodograms, and folded radial velocities for seven of the objects. Time-series photometry, and additional identification spectra appear in subsequent figures.

3.1. PBC J0325.6–0820

This X-ray source is listed in the second Palermo *Swift*-BAT hard X-ray catalog (Cusumano et al. 2010), and was identified spectroscopically as a CV by Parisi et al. (2014). It is also known as 1RXS J032540.0–081442.

The mean spectrum (Figure 2) shows Balmer and He I emission lines, and He II $\lambda 4686$ less than

³<http://mdm.kpno.noao.edu/index/Instrumentation.html>

half the strength of $H\beta$. The lines are relatively narrow, with the FWHM of $H\alpha$ being about 10 \AA , or 460 km s^{-1} . An M-type absorption spectrum is evident. This is probably from the secondary, but because our signal-to-noise is insufficient to measure absorption radial velocities, it could be from an interloper or tertiary star. We could not classify the secondary accurately, but it is roughly consistent with a spectral type between M2 and M5. Decompositions with earlier types tended to oversubtract the bandhead near 6150 \AA and undersubtract the bands in the red; later types tended to oversubtract the far red end of the spectrum when the bands were matched

We have spectra from two observing runs, in 2014 January and 2014 October. The radial velocities are consistent with two different periods, $0.0872(1) \text{ d}$ and $0.0857(1) \text{ d}$, which are separated by one cycle per five days. The number of cycles in interval between the observing runs is unknown, but the periods near 0.0872 d are constrained to be

$$P = \frac{263.324 \pm 0.005 \text{ d}}{3020 \pm 10},$$

where the denominator is an integer. The radial velocity amplitude in January was $112 \pm 12 \text{ km s}^{-1}$, but increased to $178 \pm 7 \text{ km s}^{-1}$ in October, so in Figure 2 we distinguish the two runs’ velocities with different symbols. The physical significance of the change is unclear.

We also obtained time-series photometry of PBC J0325.6–0820 on three consecutive nights in 2013 December. The light curves in Figure 4 show a wave of amplitude $\lesssim 0.1 \text{ mag}$ that produces a best period of $125.0 \pm 0.5 \text{ minutes}$ ($0.0868 \pm 0.0003 \text{ d}$) in the combined power spectrum. This is consistent with and favors the larger of the two alternative spectroscopic periods.

As noted above, the M-dwarf contribution could not be constrained precisely, but we used the Monte Carlo procedure described in Paper I to loosely constrain the system’s distance, on the assumption that the light does arise from the secondary. Choosing the spectral type from a uniform distribution between M2 to M6, and adopting liberal uncertainties for the secondary’s mass and flux contribution, yielded a distance of $400 (+170, -160) \text{ pc}$. Most CVs in this period range do not show an obvious secondary star in their spectrum, so this is likely to be a rather low-luminosity system.

3.2. Swift J0503.7–2819

We selected Swift J0503.7–2819 from the 70-month *Swift*-BAT all-sky hard X-ray survey (Baumgartner et al. 2013), and identified its counterpart as a bright, variable X-ray source in *Swift* XRT images of the field, and as a UV bright star in the *Swift* UVOT. This object is also known as 1RXS J050350.6–282324 and 1WGA J0503.8–2823.

The mean spectrum of Swift J0503.7–2819 (Figure 2) shows strong H, He I, and He II lines on a blue continuum, with He II $\lambda 4686$ roughly equal in strength to $H\beta$. The $H\alpha$ line has an equivalent

width (EW) of $\approx 55 \text{ \AA}^4$. A search for radial-velocity periodicities in $\text{H}\alpha$ was inconclusive, but the He I and He II lines showed a stronger modulation, so we adopted an average of the He I $\lambda 5876$ and He II $\lambda 4686$ velocities for the period analysis. They showed a strong periodicity near 81 minutes, but with ambiguity in the daily cycle count. Figure 5 shows a phase-binned greyscale representation of the spectra at the 81-minute period; the strong velocity modulation is especially clear in He II $\lambda 4686$ and $\lambda 5411$. However, the lines do not show the asymmetric, shifting wings typical of an AM Her star, or polar.

We obtained time-series photometry of Swift J0503.7–2819 on five nights in 2013 December and 2014 January, as shown in Figure 6. A power spectrum of the combined data shows three clear peaks, at $4896 \pm 4 \text{ s}$, $2449 \pm 1 \text{ s}$, and $975.2 \pm 0.2 \text{ s}$. The first two signals are undoubtedly the orbital period and its harmonic, corresponding to $P_{\text{orb}} = 0.05667 \pm 0.00005 \text{ d}$, or 81.60(7) min, which agrees with the favored spectroscopic value in Table 3, and resolves the ambiguity in the spectroscopic cycle count. The 975.2 s signal could be the spin period of the WD, which would make Swift J0503.7–2819 another rare example of an IP below the (orbital) period gap.

3.3. Swift J0525.6+2416

Also known as 1RXS J052523.2+241331, the spectroscopy of Swift J0525.6+2416 showed He II $\lambda 4686$ stronger than $\text{H}\beta$, suggesting a magnetic CV identification (Torres et al. 2007; Masetti et al. 2012). Bernardini et al. (2015) discovered a 226.3 s X-ray oscillation in *XMM-Newton* data from this source, establishing it as an IP. No other variability was detected in the 8.8 hr X-ray observation. In addition, Bernardini et al. (2015) rejected previous evidence for an optical eclipse in Swift J0525.6+2416 (Ramsay 2009) as being due to a telescope tracking problem.

We have obtained 20.5 hours of time-series photometry on Swift J0525.6+2416 over four nights in 2013 and 2014. The best of these optical light curves, using a *V* or BG38 filter, are shown in Figure 7. The longest is 9.6 hr and contains no eclipse. While showing variability on a variety of time scales between $\sim 500 \text{ s}$ and $\sim 6 \text{ hr}$, the optical data do not display the secure 226.3 s X-ray period, which should be detected easily if its amplitude were the same as in soft X-rays, $\approx 10\%$. Figure 7 shows the power spectrum of the 9.6 hr BG38 time series, in which any signal at 226.3 s is within the noise, and has a semi-amplitude of $\lesssim 0.004 \text{ mag}$, or a pulsed fraction of $\lesssim 0.37\%$. Bernardini et al. (2015) concluded from its energy dependence that the X-ray pulse modulation is due to photoelectric absorption in the preshock-accretion flow. Possibly most of the visible light is coming from a larger region.

⁴In this paper, we assign positive equivalent widths to emission features.

3.4. Swift J0614.0+1709

We identified this source from Baumgartner et al. (2013) as the the brightest one in XRT images of the field. Only one optical spectrum of Swift J0614.0+1709 was obtained, in the blue region, which displays higher order Balmer lines and He II $\lambda 4686$ comparable in strength to $H\beta$ (Figure 8a), identifying it as a probable magnetic CV.

Time-series photometry on three consecutive nights (Figure 9) shows a clear pair of beating periods, 1529.8(9) s and 1412.3(9) s. In addition, the difference frequency between these appears in the power spectrum as a peak at 5.00(5) hr. We interpret the 1412 s period as the spin period and the 5.00 hr period as the orbital period. (Examining the power spectrum in Figure 9, 1-day aliases of these values are an alternative possibility: 1390 s and 4.15 hr.) The 1530 s period is the strongest signal, which corresponds to the beat between the spin and orbit frequencies. When seen in X-rays in intermediate polars, this phenomenon is attributed to diskless accretion, or else to part of the accretion stream passing over the disk and coupling directly to the magnetosphere (Hellier 1993). The beat period is then due to reprocessing of the spin signal by material fixed in the orbiting frame of the system.

3.5. Swift J0623.9–0939

We identified this source from Baumgartner et al. (2013) as the the brightest one in XRT images of the field. It corresponds to 1RXS J062406.90–093815. Only one optical spectrum of Swift J0623.9–0939 was obtained (Figure 8b), which shows Balmer lines, He I and He II $\lambda 4686$, identifying it as a CV. A single 5.3 hr time series on this bright, $V \approx 14$ object, obtained during partly cloudy weather, shows flickering typical of a CV, but no obvious period. Additional data are needed to characterize this system.

3.6. PBC J0706.7+0327

This X-ray source is listed in the second Palermo *Swift*-BAT hard X-ray catalog (Cusumano et al. 2010), and also in Baumgartner et al. (2013) as Swift J0706.8+0325. It was identified spectroscopically as a CV by Parisi et al. (2014). It is also known as 1RXS J070648.8+032450.

The PPMXL catalog (Roeser et al. 2010) gives a proper motion of $[\mu_X, \mu_Y] = [-68, -43]$ mas yr^{-1} for the ≈ 17 mag optical counterpart. At 100 pc, this corresponds to a transverse velocity of 40 km s^{-1} , which suggests that the distance is less than a few hundred pc.

The mean spectrum (Figure 2) shows strong, relatively narrow lines, with broad wings. He II $\lambda 4686$ is present but weaker than $H\beta$. The $H\alpha$ emission velocities define an unambiguous period near 102 minutes, with a very large amplitude of 300 km s^{-1} . The line profiles in the phase-averaged

greyscale (Figure 5) show a narrow, low-amplitude component and a more diffuse, high-amplitude component nearly in antiphase. This is typical of polars, in which accretion occurs through a magnetically-channeled funnel onto a synchronously-rotating WD, without an accretion disk.

We obtained a single night of time-series photometry on PBC J0706.7+0327 (Figure 11), which supports the AM Her classification. It shows two large-amplitude spikes per rotation, such that the peak in the power spectrum appears at half the orbital period. The spiky, flaring nature of this light curve resembles that of the remarkable and enigmatic IGR J19552+0044 (Paper I), which is likely to be a polar, or perhaps an asynchronous polar (Bernardini et al. 2013). In PBC J0706.7+0327, the spectroscopic and photometric periods are identical to within the $\sim 2\%$ uncertainty on the latter.

3.7. Swift J0717.8–2156 and Swift J0749.7–3218

Both of these objects from Baumgartner et al. (2013) were identified as the brightest sources in XRT images of their respective fields, and as faint blue objects in the UVOT. The first corresponds to 1RXS J071748.9–215306. Spectra were obtained showing $H\alpha$ and $H\beta$ emission, as well as faint lines of He I, identifying them as likely CVs (Figure 8c,d). We do not have any time-series data on Swift J0717.8–2156 or Swift J0749.7–3218, which would be needed to further characterize their nature.

3.8. Swift J0820.6–2805

We selected Swift J0820.6–2805 from Baumgartner et al. (2013), and identified its counterpart as a bright, variable X-ray source in *Swift* XRT images of the field, and as a UV bright star in the *Swift* UVOT. This object is also known as 1RXS J082033.6–280457. It was also listed in Cusumano et al. (2010), and was identified as a CV by Parisi et al. (2014), who showed a spectrum having prominent lines of H, He I, and He II.

We were only able to obtain the brief light curves displayed in Figure 12. Although a possible peak in the power spectrum is present at 2485 ± 50 s on one night, we regard this as only a candidate for a spin period because the light curve covers only five cycles of the oscillation, so it could just be flickering. Thus, the IP (DQ Her) classification is tentative.

3.9. Swift J0939.7–3224

This source is associated with 1RXS J093949.2–322620 in Baumgartner et al. (2013). We identified it from XRT and UVOT images. Nearly all our spectral data on Swift J0939.7–3224 are from the 1.3m telescope in 2015 March. The mean spectrum (Figure 2) shows a strong, blue

continuum with relatively weak emission lines – the emission EW of $H\alpha$ is $\approx 22 \text{ \AA}$ – suggesting that the accretion disk is optically thick and the luminosity relatively high.

The $H\alpha$ radial velocities are modulated with an 8.5-hour period. Because of hour-angle constraints at the very southerly declination, the choice of daily cycle count is not entirely unambiguous, but the velocity modulation is defined well enough that the Monte Carlo test from Thorstensen & Freed (1985) gives a discriminatory power of over 95% and a correctness likelihood near unity. Despite the long orbital period, we see no clear sign of a secondary star in the mean spectrum, which corroborates the suggestion that the luminosity is relatively high.

Our time-series photometry (Figure 13) shows a possible period of 2670(7) s, but the short runs do not cover many of its cycles. Thus, we consider Swift J0939.7–3224 only a candidate for a DQ Her classification, requiring further observations, similar to the case of Swift J0820.6–2805.

3.10. 4PBC J1740.7+0603

4PBC J1740.7+0603 does not yet appear in any published paper, but we identified it from *Swift* XRT and UVOT images taken on 2014 November 4 and 5. It is included in the fourth Palermo *Swift*-BAT hard X-ray catalog⁵. We were only able to obtain brief time series on 4PBC J1740.7+0603 due to clouds and technical problems. They show typical flickering of CVs, but no obvious periods (Figure 14).

The mean spectrum (Figure 3) shows a blue continuum with strong, broad, single-peaked emission lines – the EW and FWHM of $H\alpha$ are 125 \AA and 1400 km s^{-1} , respectively. He II $\lambda 4686$ is about 1/3 the strength of $H\beta$. A period search of the $H\alpha$ velocities was inconclusive, but the He I $\lambda 5876$ and $\lambda 6678$ lines showed a low-amplitude velocity modulation near 101 minutes, with daily aliasing. The modulations in the two lines independently gave the same period and phase, within uncertainties, so the periodicity is likely to be real. However, the low signal-to-noise yielded rather poor frequency discrimination, so the daily cycle count remains ambiguous. Figure 5 shows a phase-averaged greyscale representation of the data. The $\sim 30 \text{ km s}^{-1}$ velocity modulation would not be apparent at this scale, but unfortunately other subtle phenomena (line wings, S-waves, etc.) do not appear; the absence of such corroboration suggests that the period determination should be viewed with some caution.

3.11. Swift J2124.6+0500

We selected this X-ray source from Baumgartner et al. (2013). It is also listed in Cusumano et al. (2010) as PBC J2124.5+0503, and was identified spectroscopically as a CV by Parisi et al. (2014).

⁵http://bat.ifc.inaf.it/100m_bat_catalog/100m_bat_catalog_v0.0.htm

The mean spectrum (Figure 3) shows a strong, blue continuum with relatively weak emission lines, characteristic of a novalike variable. The EW of $H\alpha$ is only 17 Å, and its FWHM is 650 km s⁻¹. The He I lines are rather weak, but He II $\lambda 4686$ is strong, and the C III/N III blend at $\lambda 4640$ is about half the strength of $H\beta$. On the basis of the latter line features, and its bright continuum, Halpern (2013) originally suggested an LMXB classification for Swift J2124.6+0500. However, its high Galactic latitude ($b = -30.^\circ 5$) and absence of brighter historical X-ray detections favor a CV interpretation.

As is often the case with novalike variables, the radial velocity modulation is ragged, despite ample counting statistics. However, our data do show a significant modulation at 20.1 hours, which is consistent across many observing runs. Daily aliases are possible but unlikely. The cycle count between observing runs is not determined well, with several reasonable fits spaced in frequency by approximately one cycle per 57 days.

3.12. Swift J2341.0+7645

Swift J2341.0+7645 was identified spectroscopically as a CV by Lutovinov et al. (2012); it corresponds to 1RXS J234015.8+764207. The mean spectrum (Figure 3) shows strong Balmer, He I, and He II emission lines, with He II $\lambda 4686$ (which is near the edge of the spectral range, these data having been taken with a smaller detector than the others) comparable in strength to $H\beta$. The averaged line profiles have a narrow core and broad wings. The $H\alpha$ radial velocities show a clear periodicity at 3.7 hours. The line core velocities (measured using convolution with a narrow Gaussian) and the line wing velocities (measured using Gaussians separated by ≈ 1500 km s⁻¹ give the same period, within the uncertainties; however, the line core velocities lag behind the wings by about 0.2 cycles. For the cores, the velocity semi-amplitude K is 77 ± 8 km s⁻¹, while for the wings it is 151 ± 13 km s⁻¹. The data in Table 3 and Figure 3 are for the line wings. Swift J2341.0+7645 may be a polar, but the case for this is not as strong as it is for PBC J0706.7+0327. However, we also obtained time-series photometry of Swift J2341.0+7645 on three consecutive nights using the Andor camera on the 1.3m telescope. Figure 15 shows a highly modulated signal at the spectroscopic period, and no shorter periods, which supports classification as a polar.

4. CONCLUSIONS

We identified seven new CV counterparts of *Swift*-BAT survey sources, and studied an additional six that were previously known. Two of the new identifications, Swift J0503.7–2819 (975 s) and Swift J0614.0+1709 (1412 s), are IPs based on likely spin periods detected in their photometry. The latter also shows a strong signal at 1530 s, the beat period between the spin and the 5.00 hr orbit. Another two, Swift J0820.6–2805 and Swift J0939.7–3224 have possible spin periods that need to be confirmed, 2585 s and 2670 s, respectively. The previously known source PBC J0706.7+0327

is shown to be a polar based on its two-component line profiles, high radial velocity amplitude, and large photometric variability on the same 102 minute period. Its unusual light curve resembles that of the enigmatic IGR J19552+0044 (Paper I). Swift J2341.0+7645 may be a polar based on its spectra and orbital light curve. Polarimetry could clarify its nature.

Notably, our long optical light curve of Swift J0525.6+2416 does not detect the 226 s spin period discovered in X-rays by Bernardini et al. (2015), to a sensitive limit. On the other hand, Bernardini et al. (2015) detect in X-rays the 1218 s optical spin period of 1RXS J045707.4+452751 (Swift J0457.1+4528) reported in Paper I, at a similar amplitude.

Although the small subset of *Swift*-BAT CVs studied here is not a well-defined “sample” in any quantitative sense, these results are consistent with the expectation that hard X-ray selection favors magnetic CVs, and that IPs outnumber polars in hard X-ray surveys because of their higher accretion rates, and because in polars some fraction of the accretion energy is radiated as a soft X-ray blackbody from the WD surface.

We obtained orbital periods for seven objects from radial-velocity spectroscopy and time-series photometry, the latter useful to resolve ambiguities in cycle count. These range from 81 minutes to 20.4 hours. With an orbital period of 81 minutes, Swift J0503.7–2819 can be added to the small but growing number of IPs with orbital periods below the period gap, similar to IGR J18173–2509 (92 minutes) and AX J1853.3–012 (87 minutes) from Paper I. Swift J0503.7–2819 also has the unusually large value of $P_{\text{spin}}/P_{\text{orb}} = 0.2$ and, similar to IGR J18173–2509, is another exception to the observation of Scaringi et al. (2010) that all hard X-ray-detected IPs have $P_{\text{spin}}/P_{\text{orb}} < 0.1$.

We thank Sean McGraw for obtaining the identification spectra of Swift J0614.0+1709 and Swift J0623.9–0939. We gratefully acknowledge support from NSF grant AST–1008217.

5. APPENDIX AN X-RAY PERIOD FROM RX J2015.6+3711

RX J2015.6+3711 was spectroscopically identified as a CV by Halpern et al. (2001, 2002) during a survey of the field of the γ -ray source 3EG J2016+3657. It was flagged as likely a magnetic CV because its He II $\lambda 4686$ emission line is comparable in strength to $H\beta$. It is in a region crowded with high-energy sources from soft X-rays to TeV γ -rays, including the hard X-ray source IGR J20159+3713, which corresponds to the BAT source Swift J2015.9+3715/4PBC J2015.5+3711, and the supernova remnant/pulsar wind nebula CTB 87 = G74.9+1.2. As discussed in detail by Bassani et al. (2014), the identification of the source of the hard X-rays in this region is ambiguous, principally because there is also the blazar B2013+370 only 1.7 from RX J2015.6+3711, and they are both within the hard X-ray error circle. Baumgartner et al. (2013) identify the BAT source as the blazar while Cusumano et al. (2010) identify it as the CV; neither is obviously wrong. Bassani et al. (2014) favor the blazar as the primary source above 20 keV, while considering that

the CV probably makes some contribution.

We cannot resolve this ambiguity; however we report here the discovery of a 2.00 hour period in the X-ray emission from RX J2015.6+3711, detected near the edge of an archival *Chandra* ACIS-I image of CTB 87 (ObsID 11092, Matheson et al. 2013). With a continuous exposure of 70 ks and a time resolution of 3.2 s, this observation is well suited to searching for an orbital or spin period. Figure 16 shows the light curve and power spectrum in the 0.5–2 keV band, chosen for display because the amplitude of modulation is greatest in soft X-rays. A period of 7215(31) s is clearly detected, as well as significant power at 3596(9) s, the harmonic. The origin of the harmonic power is evident in the asymmetric light curve.

The complete set of energy-resolved folded light curves from 0.5–8 keV are shown in Figure 17. The disappearance of the modulation in the harder X-rays indicates that its origin is photoelectric absorption. This effect also rules out an instrumental origin, for example, the dithering of the satellite. (The dither periods are 1000 s and 707 s in perpendicular directions; neither is commensurate with the measured 2.00 hours.) The complex shape and large amplitude of the soft X-ray light curve suggests an AM Her origin, in which the modulation is due to the varying view of the accretion stream. The absence of any shorter period in X-rays, such as would be expected from the spin of an IP, is consistent with this conclusion. Unfortunately, we do not yet have enough optical time-series data on RX J2015.6+3711 for comparison.

REFERENCES

- Alam, S., Albareti, F. D., Allende Prieto, C., et al. 2015, *ApJS*, 219, 12
- Bassani, L., Landi, R., Malizia, A., et al. 2014, *A&A*, 561, A108
- Baumgartner, W. H., Tueller, J., Markwardt, C. B., et al. 2013, *ApJS*, 207, 19
- Bernardini, F., de Martino, D., Mukai, K., et al. 2013, *MNRAS*, 435, 2822
- Bernardini, F., de Martino, D., Mukai, K., et al. 2015, *MNRAS*, 453, 3100
- Bessell, M. S. 1990, *PASP*, 102, 1181
- Cusumano, G., La Parola, V., Segreto, A., et al. 2010, *A&A*, 524, A64
- Halpern, J. P. 2013, *ATel*, 5208
- Halpern, J. P., Eracleous, M., Mukherjee, R., & Gotthelf, E. V. 2001, *ApJ*, 551, 1016
- Halpern, J. P., Eracleous, M., Mukherjee, R., & Gotthelf, E. V. 2002, *ApJ*, 572, 693
- Hellier, C. 1993, *PASP*, 105, 966
- Henden, A. A., Levine, S. E., Terrell, D., Smith, T. C., & Welch, D. 2012, *JAVSO*, 40, 430

- Hög, E., Fabricius, C., Makarov, V. V., et al. 2000, *A&A*, 355, L27
- Horne, K. 1986, *PASP*, 98, 609
- Lutovinov, A. A., Burenin, R. A., Revnivtsev, M. G., et al. 2012, *AstL*, 38, 281
- Masetti, N., Parisi, P., Jiménez-Bailón, E., et al. 2012, *A&A*, 538, A123
- Matheson, H., Safi-Harb, S., & Kothes, R. 2013, *ApJ*, 774, 33
- Monet, D. G., Levine, S. E., Canzian, B., et al. 2003, *AJ*, 125, 984
- Parisi, P., Masetti, N., Rojas, A. F., et al. 2014, *A&A*, 561, A67
- Ramsay, G. 2009, *ATel*, 2093
- Roeser, S., Demleitner, M., & Schilbach, E. 2010, *AJ*, 139, 2440
- Scaringi, A., Bird, A. J., Norton, A. J., et al. 2010, *MNRAS*, 401, 2307
- Schneider, D., & Young, P. 1980, *ApJ*, 238, 946
- Shafter, A. W. 1983, *ApJ*, 267, 222
- Thorstensen, J. R., & Halpern, J. 2013, *AJ*, 146, 107 (Paper I)
- Thorstensen, J. R., & Freed, I. W. 1985, *AJ*, 90, 2082
- Thorstensen, J. R., Patterson, J., Thomas, G., & Shambrook, A. 1996, *PASP*, 108, 73
- Torres, M. A. P., Steeghs, D., Jonker, P. G., et al. 2007, *ATel*, 1286
- Zacharias, N., Finch, C. T., Girard, T. M., et al. 2013, *AJ*, 145, 44

Table 1. Stars Observed

Name	R.A. ^a (h m s)	Decl. ^a (° ' ")	V	Ref ^b	Data ^c	Class ^d	P (s)	Ref ^e
PBC J0325.6–0820	03 25 39.43	–08 14 42.8	18.3	S	S, T	N		
Swift J0503.7–2819	05 03 49.25	–28 23 08.8	18.1	S	I, S, T	DQ	975.2(2)	1
Swift J0525.6+2416	05 25 22.75	+24 13 33.5	16.6	D	S, T	DQ	226.28(7)	2
Swift J0614.0+1709	06 14 12.28	+17 04 32.6	17.5	D	I, T	DQ	1412.3(9) ^f	1
Swift J0623.9–0939	06 24 06.18	–09 38 52.1	14.1	A	I, T			
PBC J0706.7+0327	07 06 48.94	+03 24 47.5	18.1	S	S, T	AM		
Swift J0717.8–2156	07 17 48.25	–21 53 01.8	18.9	S	I			
Swift J0749.7–3218	07 49 31.99	–32 15 37.1	18.5	B	I			
Swift J0820.6–2805	08 20 34.10	–28 04 58.7	17.8	D	T	DQ?	2485(50)?	1
Swift J0939.7–3224	09 39 49.65	–32 26 22.1	17.3	S	I, S, T	DQ?	2670(7)?	1
4PBC J1740.7+0603	17 40 45.86	+06 03 51.1	15.9	S	I, S, T			
RX J2015.6+3711	20 15 36.96	+37 11 23.2	17.8	S	X	AM	7215(31)	3
Swift J2124.6+0500	21 24 12.44	+05 02 43.6	12.7	S	S	N		
Swift J2341.0+7645	23 40 20.65	+76 42 10.5	17.9	S	S, T	AM?		

^aCoordinates are for J2000.0 (ICRS), either from the PPMXL catalogue (Roeser et al. 2010), the Sloan Digital Sky Survey (Alam et al. 2015), or derived from astrometric fits to our own images. Estimated uncertainty is $\pm 0.''2$.

^bSource of approximate V magnitude: S = our spectrophotometry; D = our direct image; A = APASS (Henden et al. 2012), as listed in the UCAC4 (Zacharias et al. 2013); B = interpolated from Schmidt-plate magnitudes in USNO B1.0 (Monet et al. 2003).

^cTypes of data presented here: I = optical spectroscopic identification; S = time-resolved spectroscopy; T = time-series photometry; X = X-ray light curve.

^dClassifications are: N = novalike variable (pulsations not confirmed); DQ = DQ Her star or IP (evidence for pulsations); AM = AM Her star or polar.

^eReference for period P , presumed to be the spin period: (1) this paper, optical; (2) Bernardini et al. 2015, X-ray; (3) this paper, X-ray.

^fOr possibly its 1-day alias, 1390.2 s. A beat period of 1530 s is also detected.

Table 2. Radial Velocities

Star	Time	v (km s ⁻¹)	σ (km s ⁻¹)	HA (hh:mm)	Exposure (s)	Telescope
PBC J0325.6–0820	56680.6241	32	3	+00:09	600	H
PBC J0325.6–0820	56680.6314	69	3	+00:19	600	H
PBC J0325.6–0820	56680.6393	89	3	+00:31	600	H
PBC J0325.6–0820	56680.6466	80	4	+00:41	600	H
PBC J0325.6–0820	56680.6540	67	4	+00:52	600	H
PBC J0325.6–0820	56680.6845	–106	4	+01:36	600	H
PBC J0325.6–0820	56680.6918	–56	5	+01:46	600	H

Note. — Emission-line radial velocities. The time given is the barycentric Julian date of mid-integration, minus 2,440,000.0, on the UTC system. The hour angle is at the start of the exposure. The telescope code is M for McGraw-Hill 1.3m, and H for Hiltner 2.4m. (This table is available in its entirety in machine-readable and Virtual Observatory (VO) forms in the online journal. A portion is shown here for guidance regarding its form and content.)

Table 3. Fits to Radial Velocities

Data set	T_0^a	P_{spec} (d)	K (km s ⁻¹)	γ (km s ⁻¹)	N	σ^b (km s ⁻¹)
PBC J0325.6–0820 ^c	56685.5866(18)	0.0871933(14)	120(13)	–3(10)	37	33
Alternate	56685.589(2)	0.0856958(19)	117(14)	0(11)	37	36
Swift J0503.7–2819	56683.6266(9)	0.05662(9)	189(20)	51(14)	24	49
Alternate	56683.5779(10)	0.05356(6)	183(22)	36(15)	24	53
PBC J0706.7+0327	56681.8996(5)	0.070907(11)	303(13)	–25(9)	27	31
Swift J0939.7–3224 ^d	57107.853(4)	0.3546(9)	86(6)	70(4)	40	20
4PBC J1740.7+0603 ^e	57195.882(4)	0.07011(20)	30(9)	–34(7)	113	30
Swift J2124.6+0500	56605.091(17)	0.84913(11) ^f	115(12)	–17(9)	132	42
Swift J2341.0+7645	56548.7460(16)	0.15424(20)	151(13)	–21(8)	38	27

Note. — Parameters of least-squares fits to the radial velocities, of the form $v(t) = \gamma + K \sin [2\pi(t - T_0)/P_{\text{spec}}]$.

^aHeliocentric Julian Date minus 2,400,000. The epoch is chosen to be near the center of the time interval covered by the data, and within one cycle of an actual observation.

^bRoot-mean-square residual of the fit.

^cThe two periods reflect different choices of daily cycle count over a 5-day gap, and the excessively precise periods tabulated here reflect in turn an arbitrary choice of cycle count between observing runs. For each choice of daily cycle count, the uncertainty in the gross period is $\sim 9 \times 10^{-5}$ d. See Section 3.1 for details.

^dFit to velocities from 2015 March only.

^eVelocities are from He I emission; the daily cycle count is uncertain.

^fThe daily cycle count is reasonably secure, but there is an ambiguity at the scale of 1 cycle per 57 days.

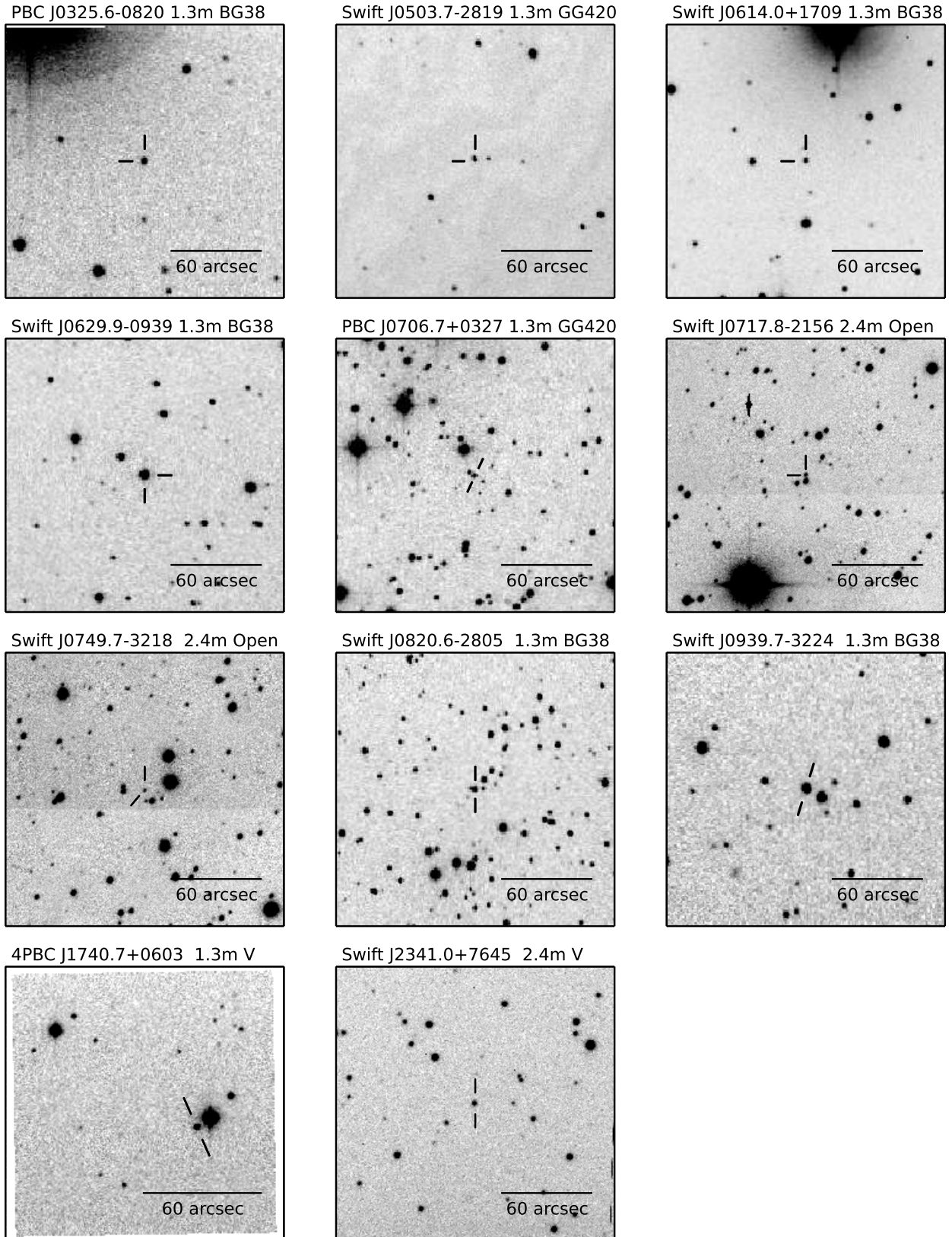


Fig. 1.— Finding charts for 11 of the objects from our 1.3m or 2.4m images. North is up, east is to the left, and the scale is indicated. The label on each chart gives the source of the image used, and the tick marks are accurately aligned with the coordinates in Table 1.

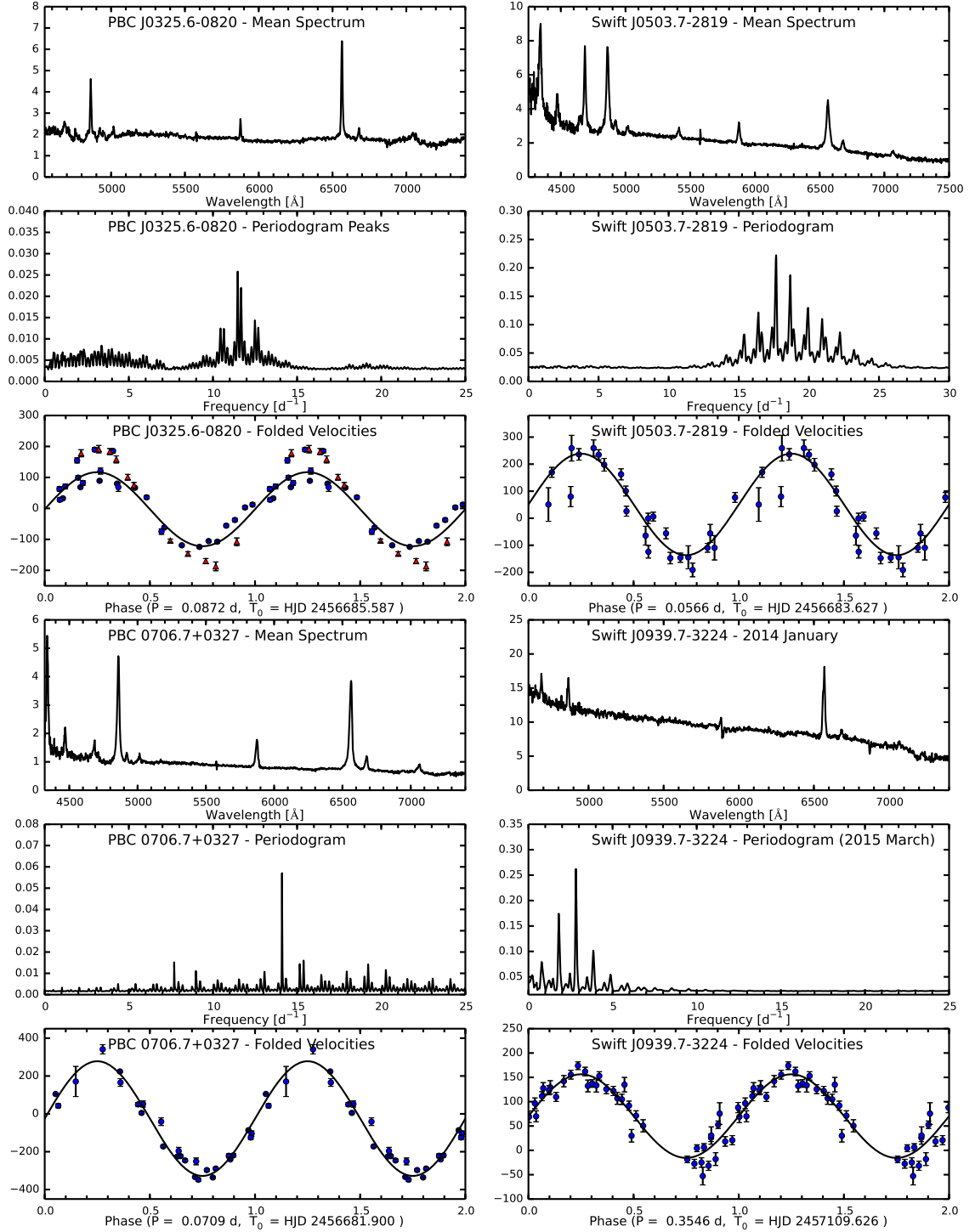


Fig. 2.— Mean spectra, periodograms, and folded velocity curves for four of the objects. The units of the vertical axes of the spectra are 10^{-16} erg cm⁻² s⁻¹ Å⁻¹; for the periodograms, the axis is unitless ($1/\chi^2$); and the radial velocities are in km s⁻¹. In the velocity curves, all data are repeated on an extra cycle for continuity, the uncertainties shown are estimated from counting statistics, and the solid curves show the best-fitting sinusoids. For PBC J0325.6–0820 (upper left), blue circles show velocities from 2014 January, and red triangles from 2014 October.

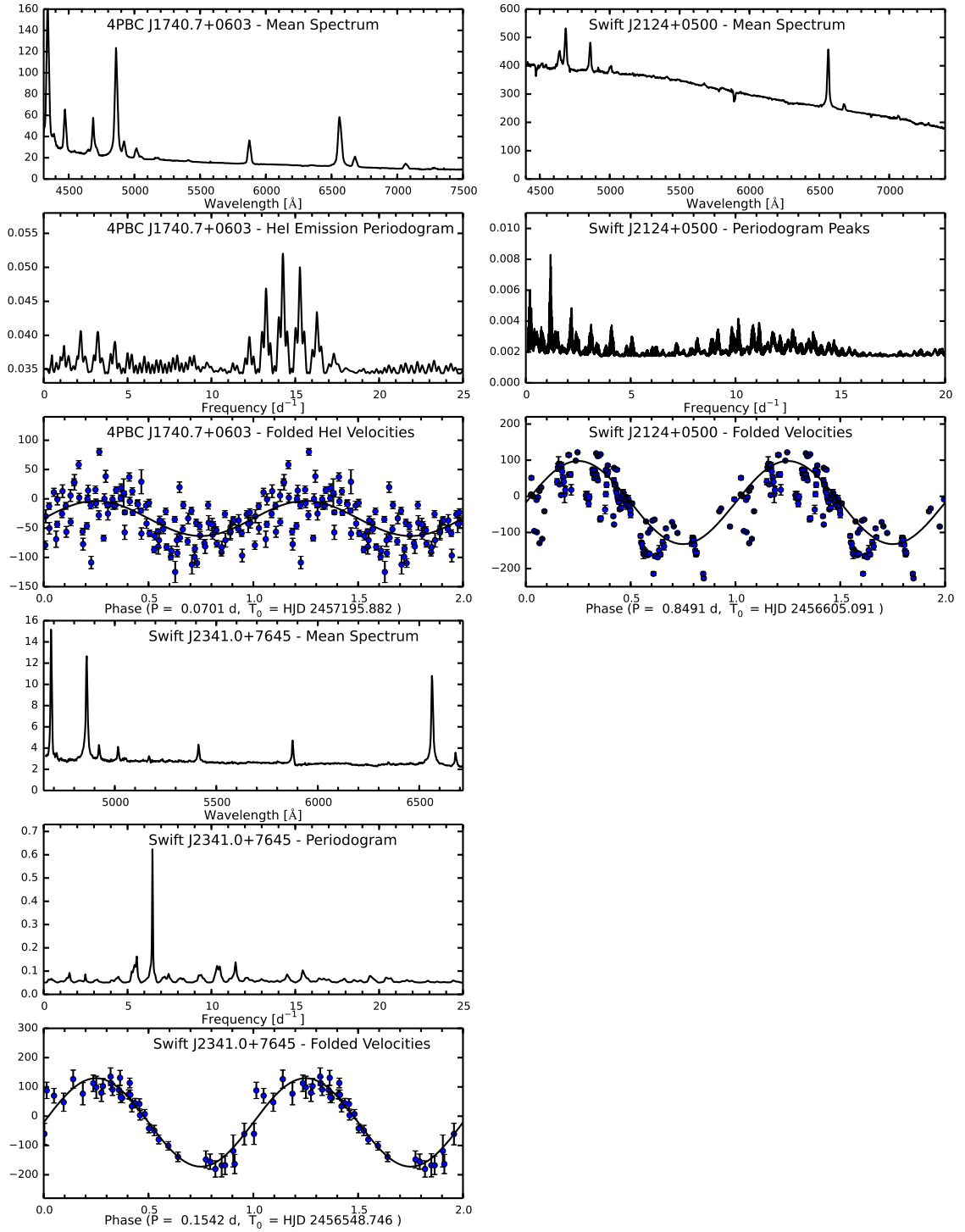


Fig. 3.— Same as Figure 2, for the remaining three objects.

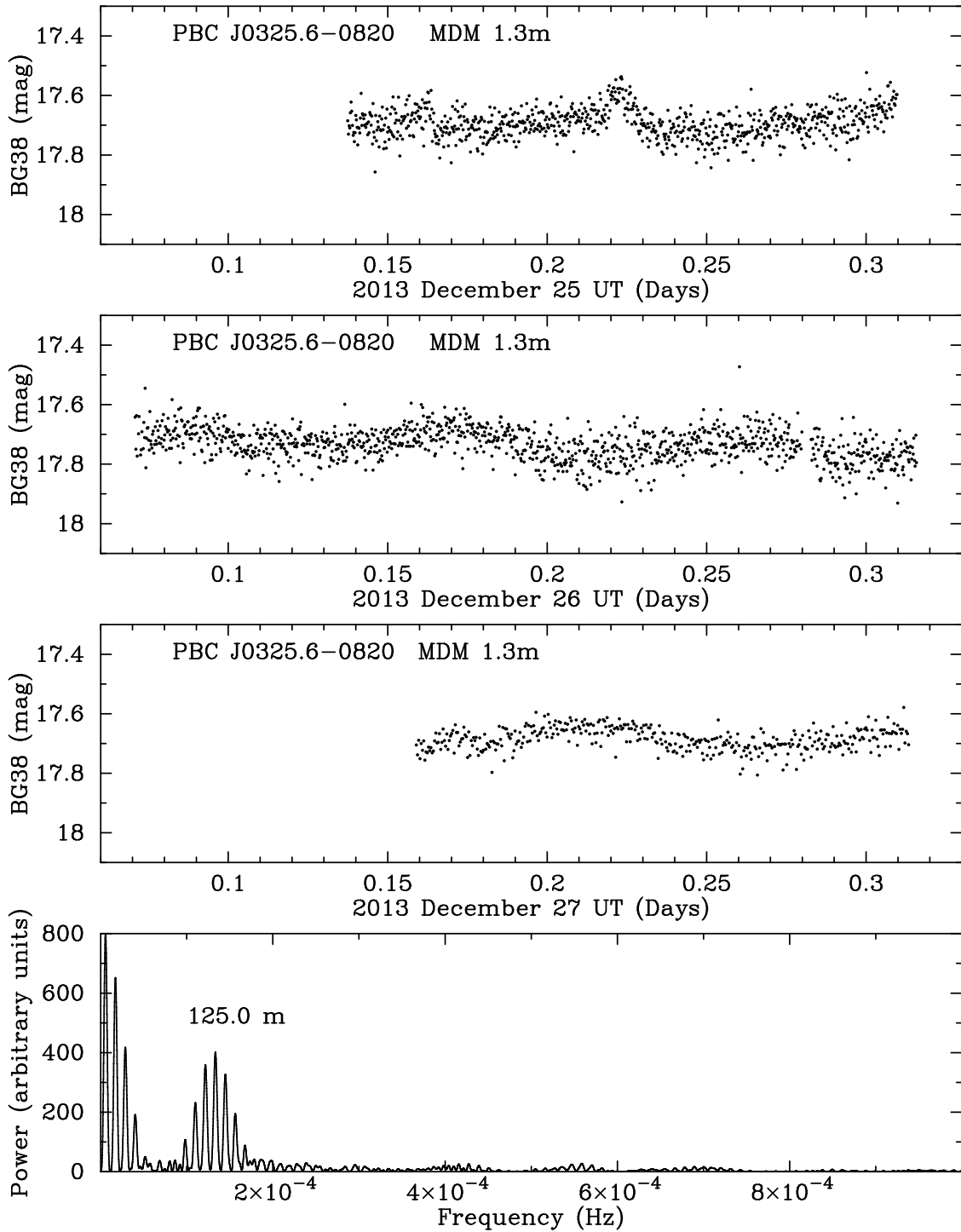


Fig. 4.— Time-series photometry of PBC J0325.6–0820 from the 1.3m. Individual exposures are 15 s (December 25, 26) or 30 s (December 27). The highest peak at 125.0 ± 0.5 minutes in the combined power spectrum agrees with one of the spectroscopic candidates.

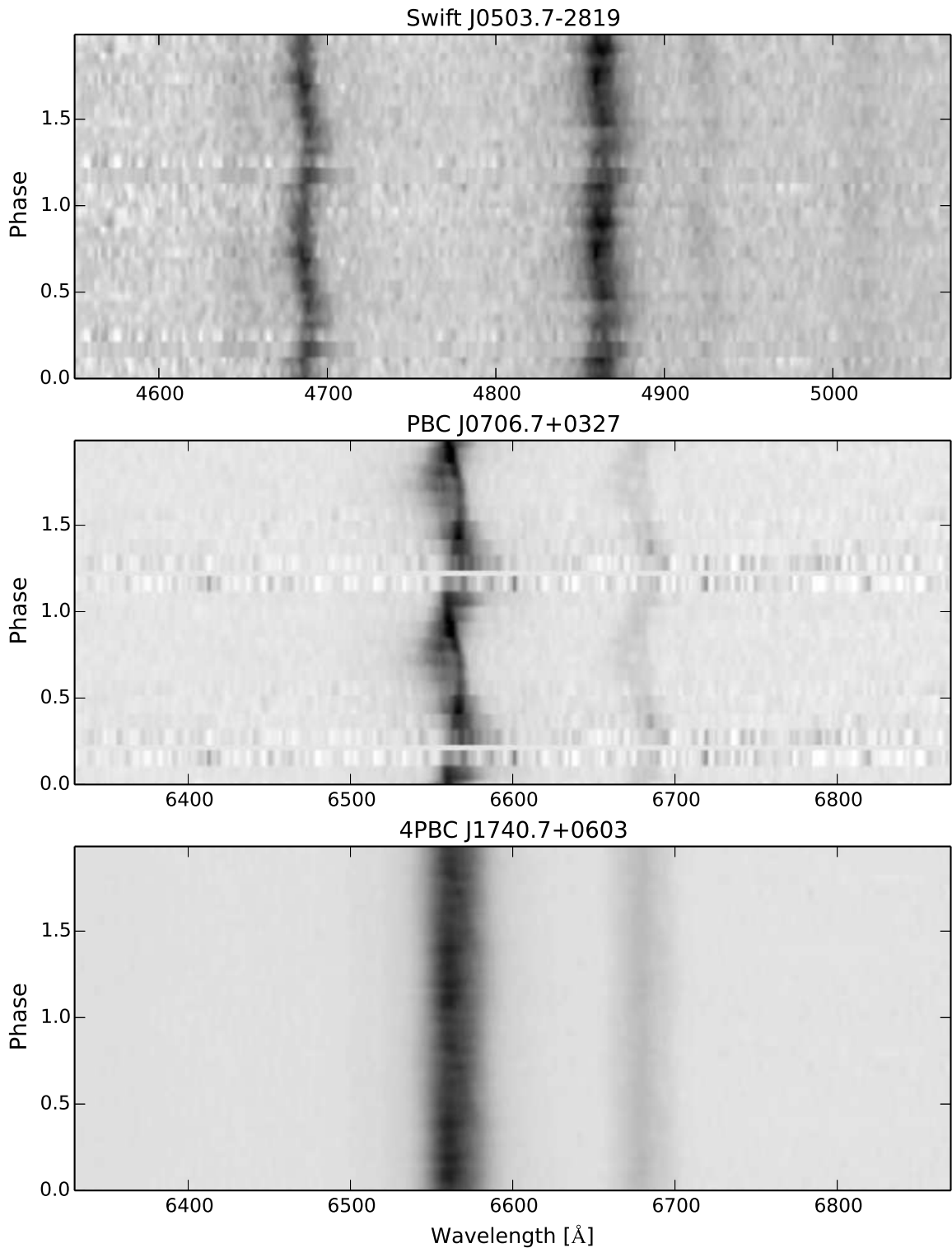


Fig. 5.— Portions of the spectra of three of the objects presented as phase-averaged greyscale images. The phases are computed using the periods and epochs in Table 3. The images are negatives, that is, darker represents more light. The spectra were rectified before phase averaging, so the continuum is forced to unity for all phases. The horizontal features in the image for PBC J0706.7+0327 are caused by poor coverage at the corresponding phase.

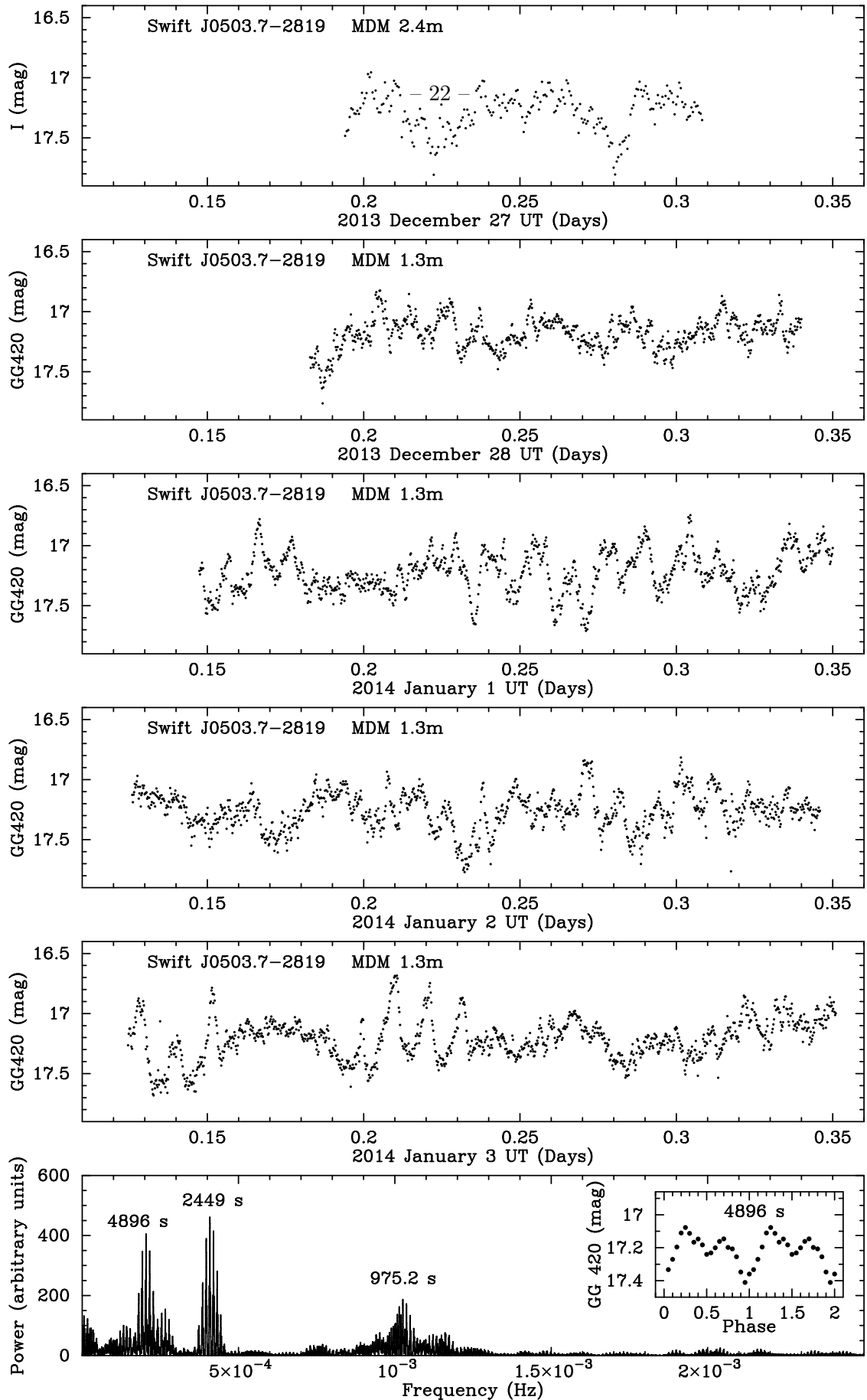


Fig. 6.— Time-series photometry of Swift J0503.7-2819. Individual exposures are 30 s on the 2.4m and 15 s on the 1.3m. The power spectrum of the combined data shows three periods, of which the longest (4896 s) agrees with the spectroscopic orbital value, and is used to fold the data in the inset. The peak at 975.2 s is possibly the spin period.

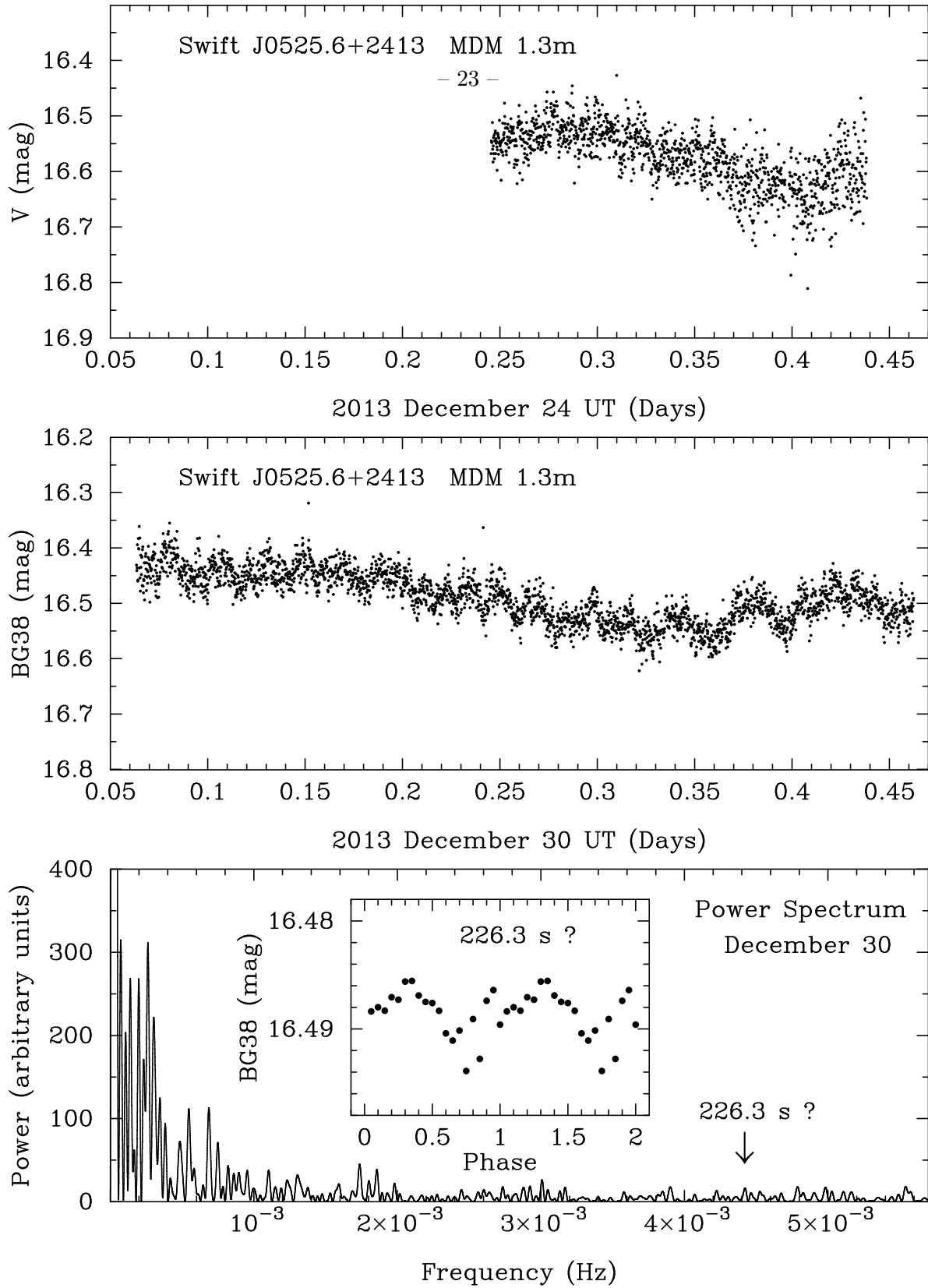


Fig. 7.— Time-series photometry of Swift J0525.6+2416. Individual exposures are 10 s. The power spectrum of the 2013 December 30 light curve does not show a significant signal at the 226.3 s period detected in X-rays (Bernardini et al. 2015). Inset: a fold at 226.3 s has a half amplitude of at most 0.004 mag.

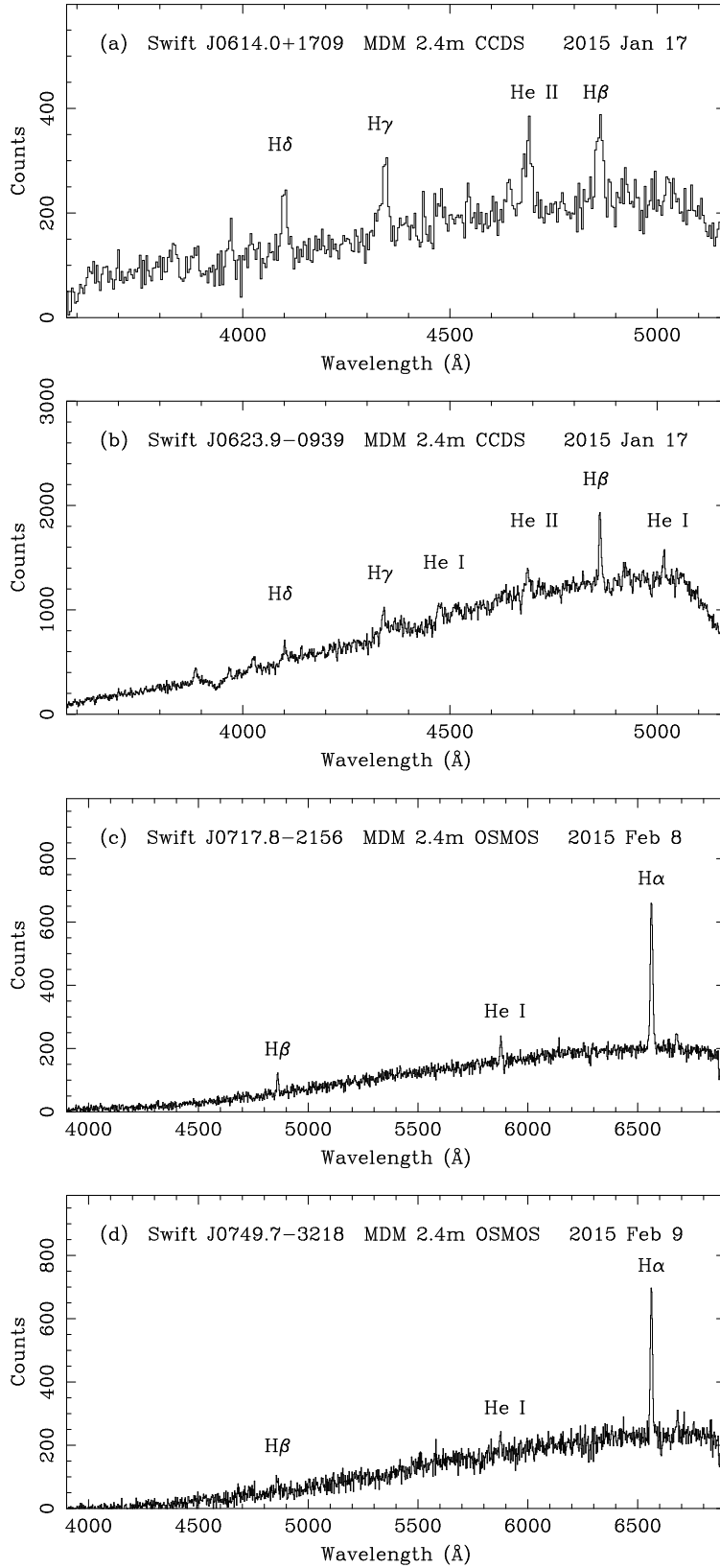


Fig. 8.— Identification spectra of four *Swift*-BAT sources obtained on the MDM 2.4m with the CCDS or OSMOS. (a) Swift J0614.0+1709. (b) Swift J0623.9–0939. (c) Swift J0717.8–2156. (d) Swift J0749.7–3218. Balmer, He I, and He II emission lines identify them as CVs. Fluxes are not calibrated.

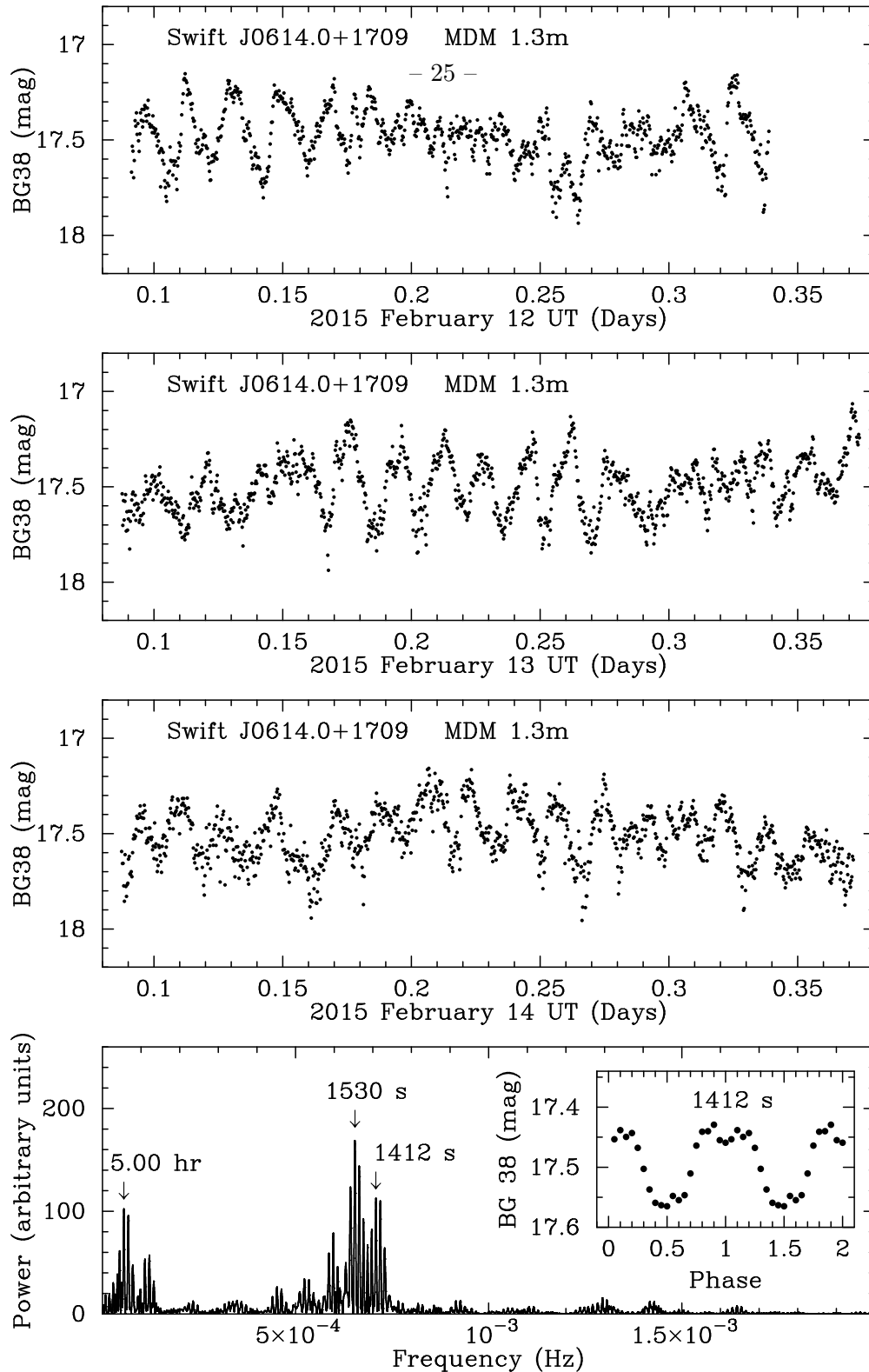


Fig. 9.— Time-series photometry of Swift J0614.0+1709. Individual exposures are 20 s. The power spectrum of the combined data shows three periods, of which the shortest (1412 s) is likely to be the spin period, the longest (5.00 hr) the orbital period, and the strongest (1530 s) the beat period between the spin and the orbit. (One-day aliases of the spin and orbit are an alternative possibility: 1390 s and 4.15 hr.) In the inset, all of the data are folded on the presumed spin period.

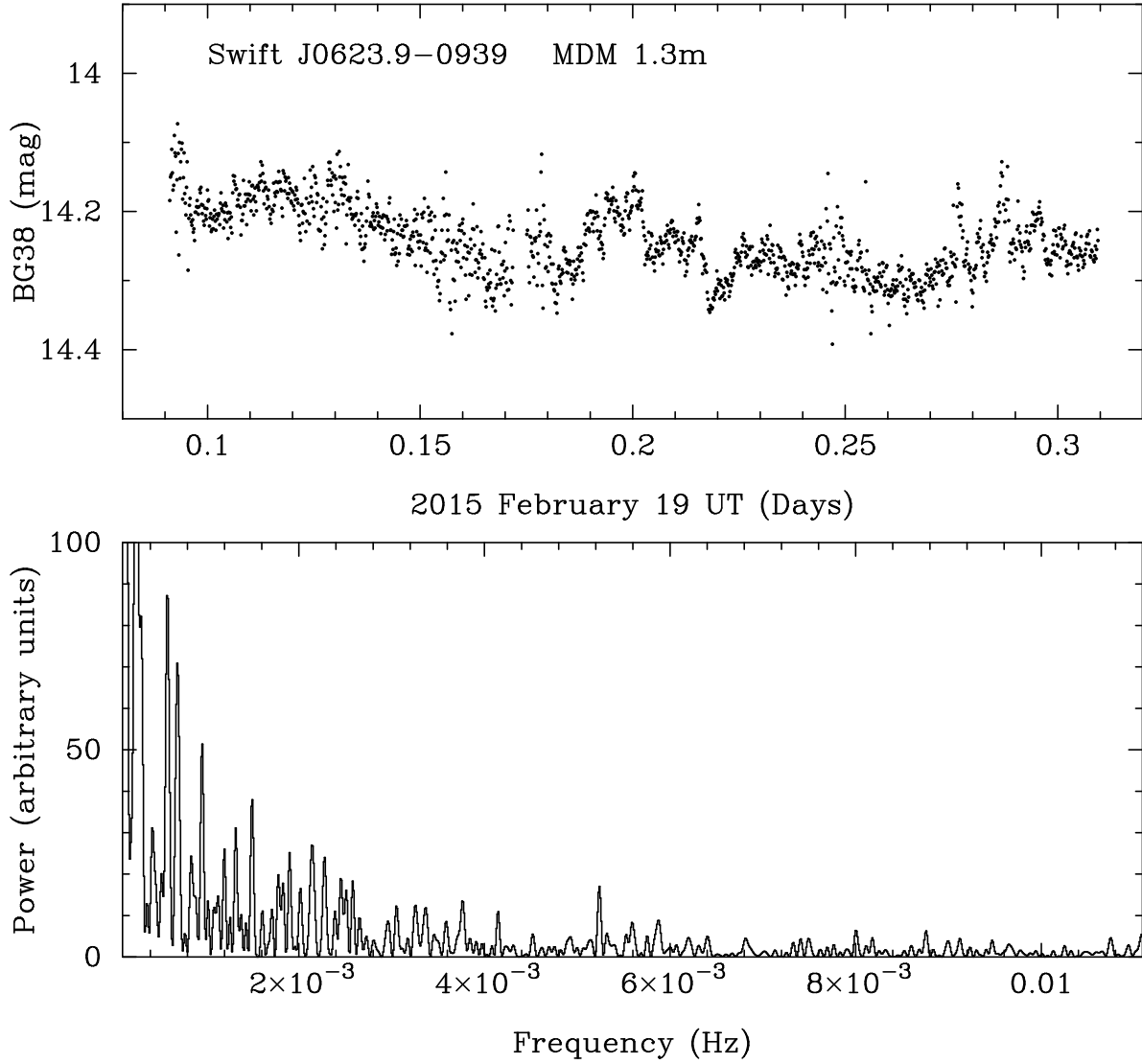


Fig. 10.— Time-series photometry of Swift J0623.9–0939. Individual exposures are 10 s. This bright object was observed under partly cloudy conditions, which is responsible for some of the scatter. There is no period evident in the power spectrum.

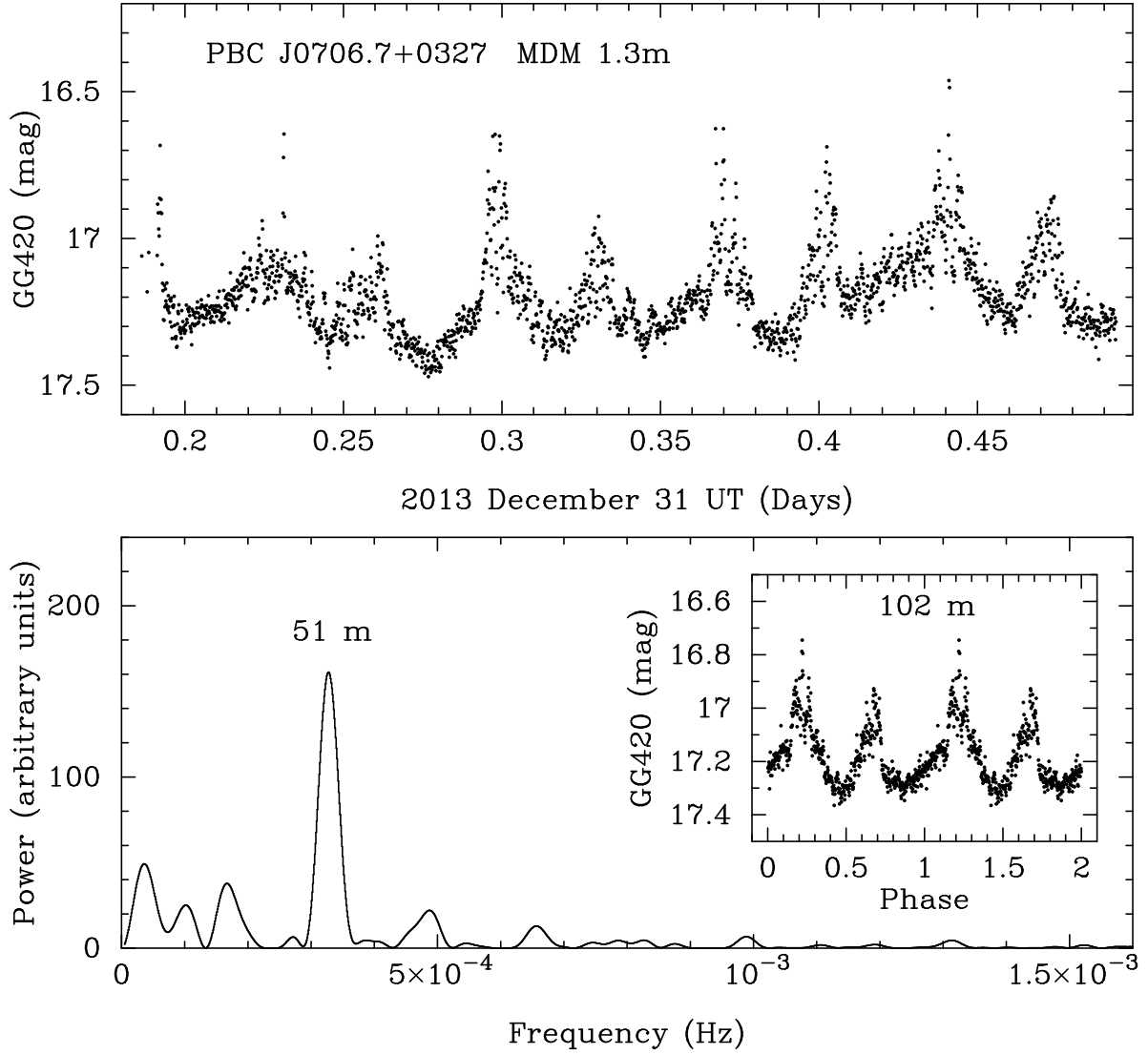


Fig. 11.— Time-series photometry of PBC J0706.7+0327 from the 1.3m. Individual exposures are 10 s. The peak in the power spectrum at 51 minutes corresponds to half the spectroscopic orbital period. The inset shows the mean double-peaked light curve folded on the 102 minute orbital period.

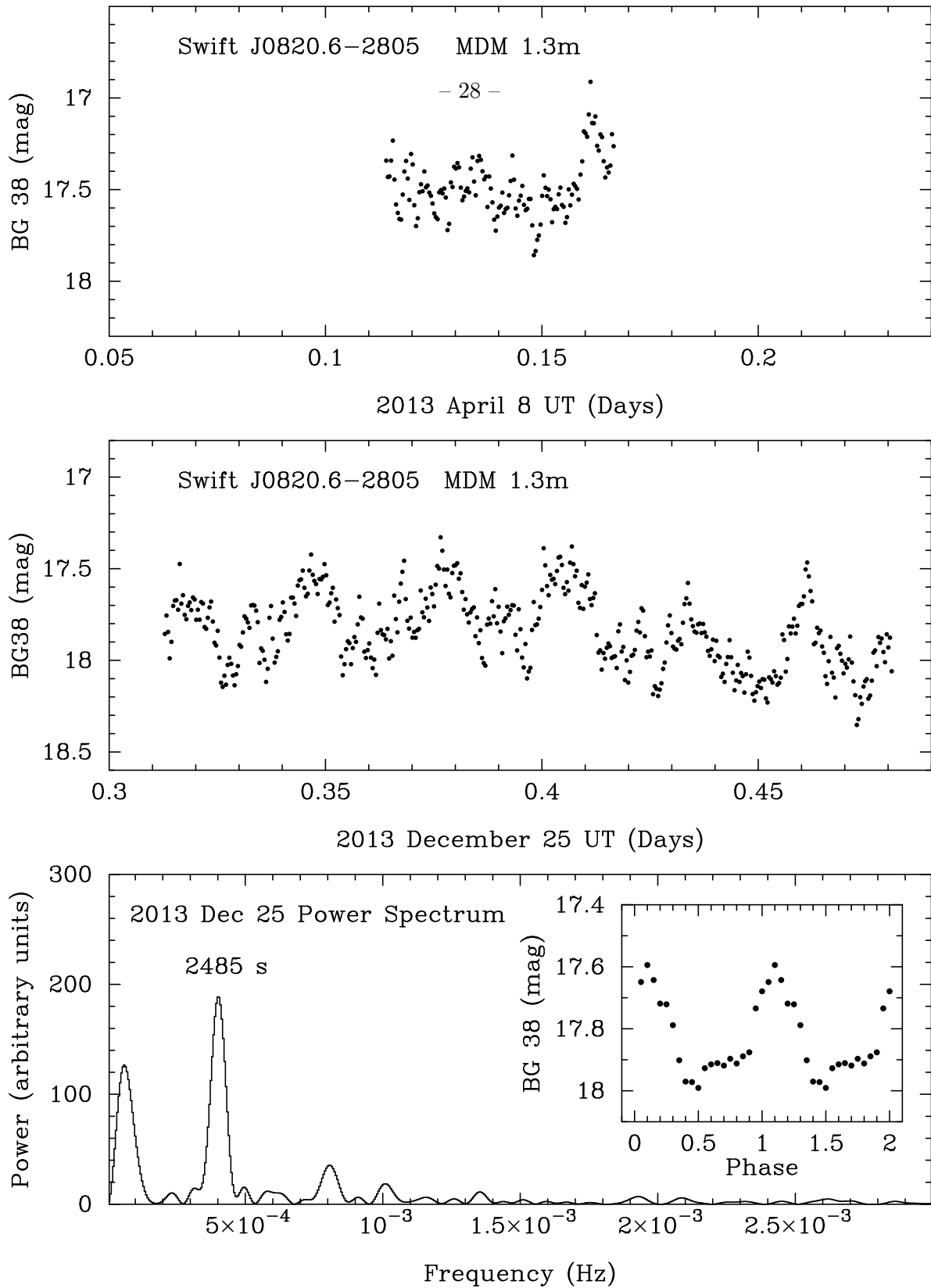


Fig. 12.— Time-series photometry of Swift J0820.6-2805 from the 1.3m. Individual exposures are 30 s. The inset shows the mean light curve from 2013 December 25 folded on the tentative 2485 ± 50 s period.

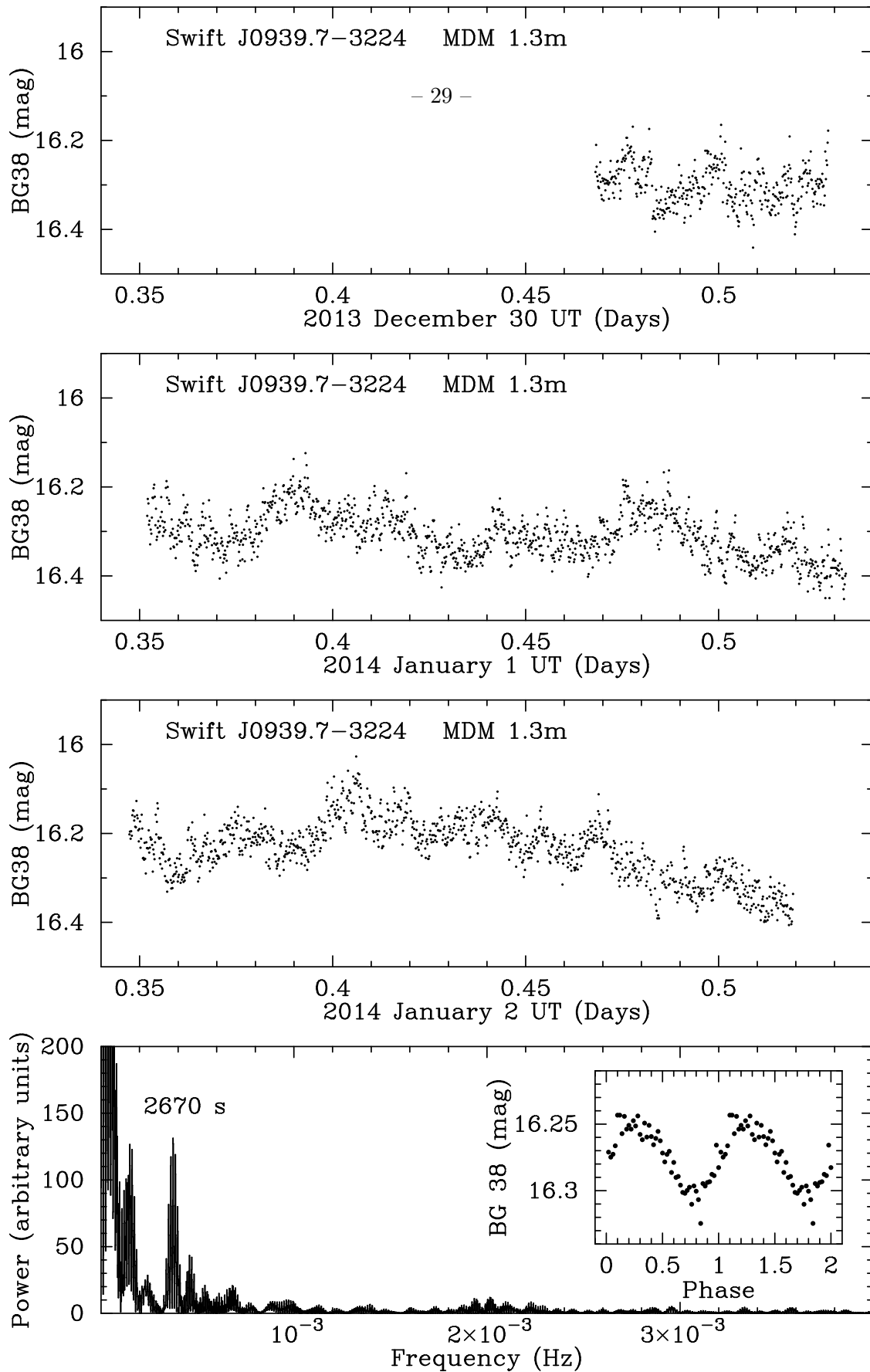


Fig. 13.— Time-series photometry of Swift J0939.7-3224 from the 1.3m. Individual exposures are 10 s. The inset shows the mean light curve folded on the tentative 2670 ± 7 s period.

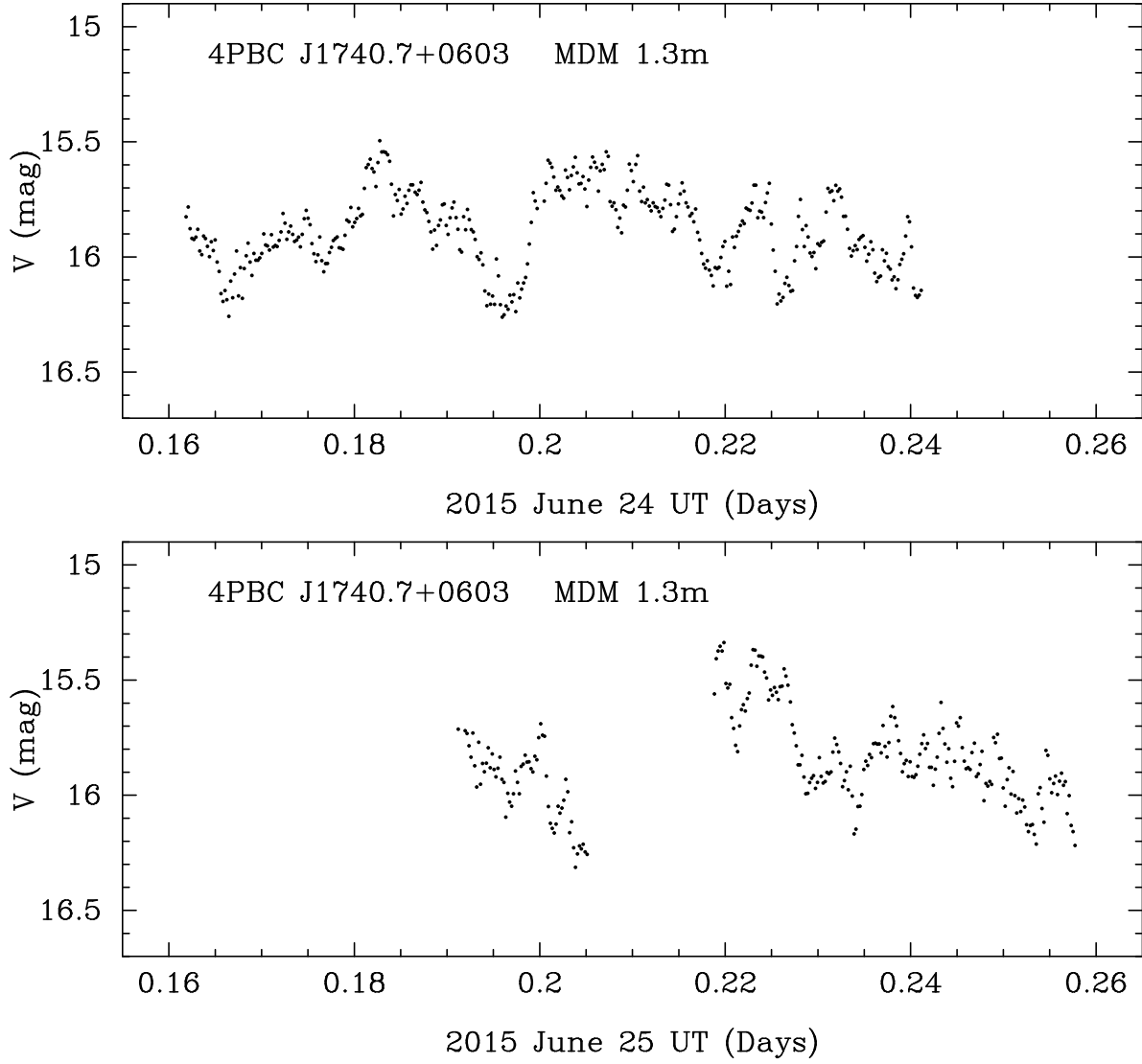


Fig. 14.— Time-series photometry of 4PBC J1740.7+0603 in the V filter from the 1.3m. Individual exposures are 15 s. The magnitude is calibrated with respect to the adjacent bright star seen in Figure 1, Tyc 427-1298-1 which has $V = 11.53 \pm 0.12$ (Høg et al. 2000).

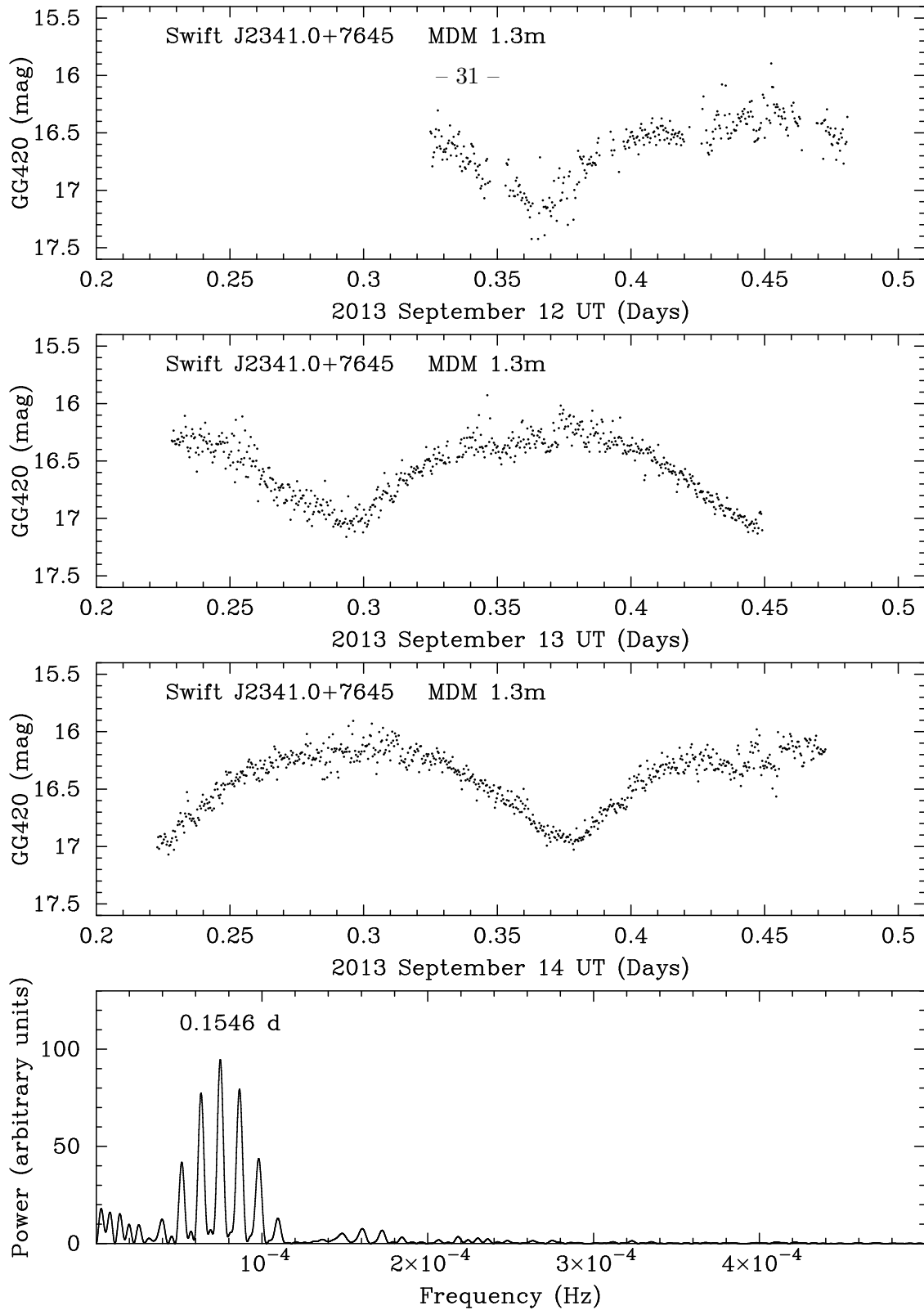


Fig. 15.— Time-series photometry of Swift J2341.0+7645 using the Andor camera on the 1.3m. Individual exposures are 30 s. The photometric period in the power spectrum, 0.1546(6) days, is in agreement with the spectroscopic period.

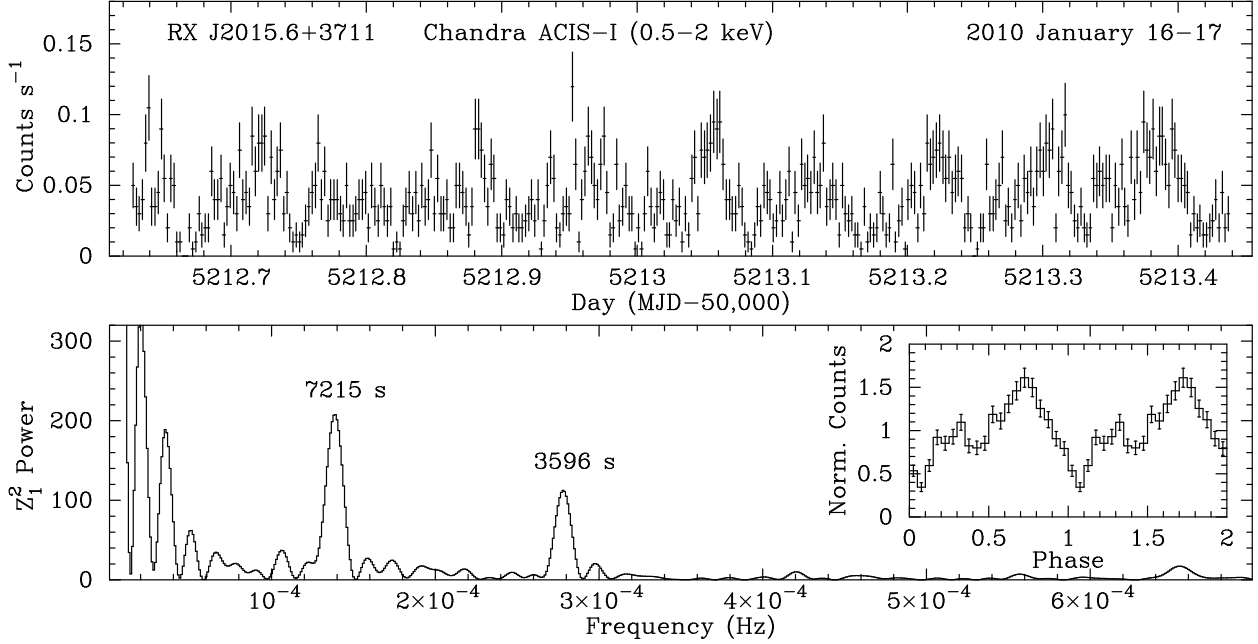


Fig. 16.— *Chandra* (ObsID 11092) light curve of RX J2015.6+3711 in soft X-rays. Top: The 0.5–2 keV X-rays in 200 s bins. Bottom: A Z_1^2 periodogram (Rayleigh test) of the 0.5–2 keV X-rays, revealing the orbital period of 7215(31) s and its harmonic at 3596(9) s. The inset is the background subtracted and normalized 0.5–2 keV light curve folded at the orbital period. See Figure 17 for other energy ranges.

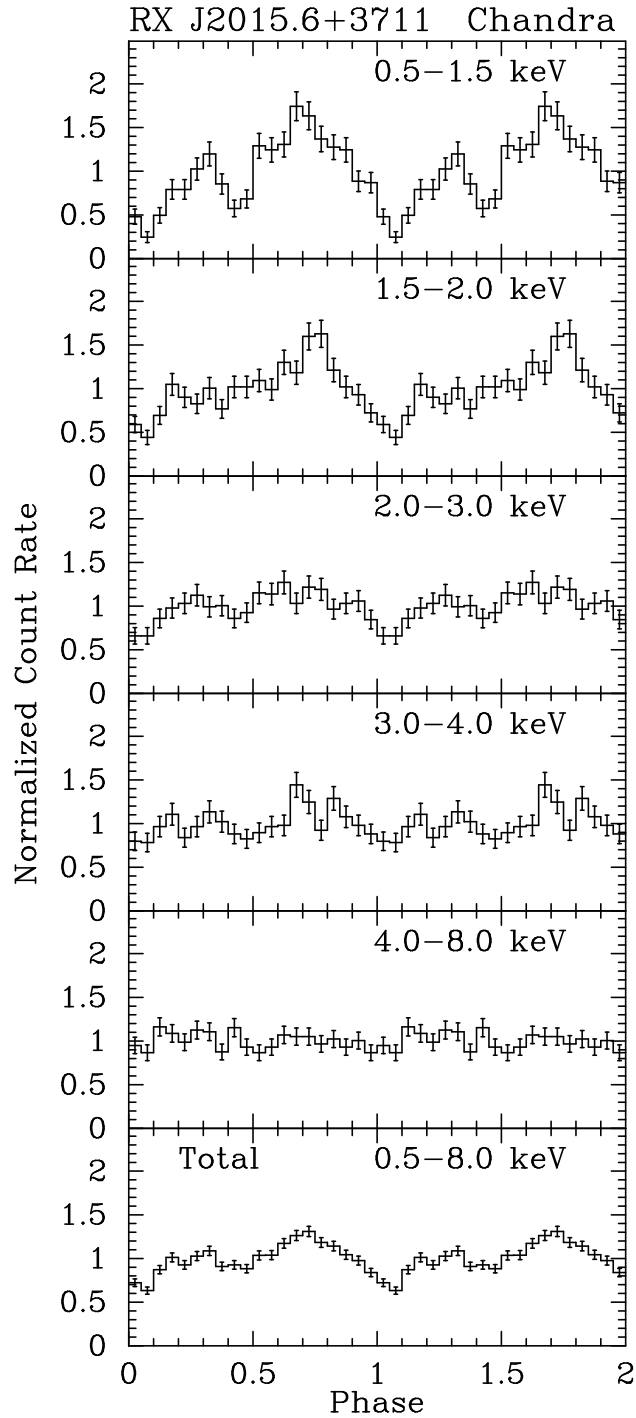


Fig. 17.— Energy-dependent folded light curves from the *Chandra* observation of RX J2015.6+3711. As in Figure 16, background from a nearby region in the image has been subtracted, and the counts per bin are normalized to 1.